Magnetic Structure of Iron Oxide Nanoparticles Using SANS

Summer School on Small Angle Neutron Scattering and Neutron Reflectometry
NIST Center for Neutron Research

K. Krycka, A. Jackson, C. Dennis

May 10 – 14 2010

Contents

1 Introduction

Heat has a profound effect on biological systems, especially cancer [1]. However, the widespread clinical application of thermal therapy [2–5] for cancer has yet to be realized despite the knowledge of its biological effectiveness, including an understanding of many of the molecular and physiologic mechanisms that give rise to its tumoricidal effects [6, 7].

Magnetic nanoparticles, offer the potential to deliver site-selective, and even cell-specific, heat to the local or microscopic environment of a tumor [3, 8]. Because the magnetic nanoparticle can also be a contrast agent for magnetic imaging [9–11] or can be labeled with an imaging ligand, there exists the possibility to quantify the deposited heat dose to the tumor [3]. Correlating heat dose with tissue temperature rise and therapeutic outcome offers the tools clinicians require to develop and use prescriptive thermal treatment plans for their patients.

When exposed to an alternating magnetic field (AMF), magnetic materials generate heat via four possible loss mechanisms: (1) hysteresis, (2) eddy current, (3) Neél paramagnetic switching, and (4) friction from Brownian rotation [12]. It is quite possible that all four mechanisms may contribute to the total heat generated by a particular magnetic sample in an AMF, but it is expected that only one or two of the mechanisms will dominate. This is determined by the properties of the magnetic material, its environment (e.g. temperature), and the magnetic field. For example, the material often chosen for biomedical applications is magnetite, Fe3O4, because it exhibits a lower toxicity than other magnetic materials while still possessing useful magnetic properties [13, 14]. For samples of this resistive oxide with dimension $\ll 1$ μm that are exposed to an AMF in the intermediate radiofrequency region (f $\sim$ 105 Hz), the heat generated by eddy current losses is likely negligible; instead, the dominant sources of heat are expected to be magnetodynamic (hysteresis, Neél switching, and frictional contributions) [15].

Successful application of this technology requires synthesis of stable colloidal suspensions of magnetite nanoparticles in biocompatible fluids (water or saline solution) that maintain their stability in biological media such as blood or plasma [16–19]. The particles must also produce a predictable and sufficient amount of heat, or specific absorption rate (SAR) measured in W g^{-1}, at modest particle concentrations (in order to limit toxicity) when exposed to AMF amplitudes that can be applied safely to large regions of tissue [20]. Thus, the surface chemistry, size, and magnetic properties of the particles must be engineered to meet demanding, even competing, performance criteria.

The process of engineering such particles requires measurement techniques that allow all relevant properties of the particles to be probed. Different preparation techniques can potentially produce materials with differing structure and behaviors on the nanometer length scale which may be crucial to understanding the differences seen in AMF response and heating rates.

Here we will study dextran coated magnetite particles which have previously been studied [21–23] in H_2O and D_2O. The expectation had been that the scattering in D_2O would be essentially similar to that in H_2O but with lowered intensity as the scattering length density of D_2O is closer to Fe_3O_4 than that of H_2O, allowing determination of the core-shell structure of the coated particles. The results (Figure 1), however, were rather different and the interpretation was that D_2O and the nanoparticle core were well matched in scattering and hence that the residual scattering was either from the dextran shell or internal magnetic structure in the nanoparticle. This interpretation

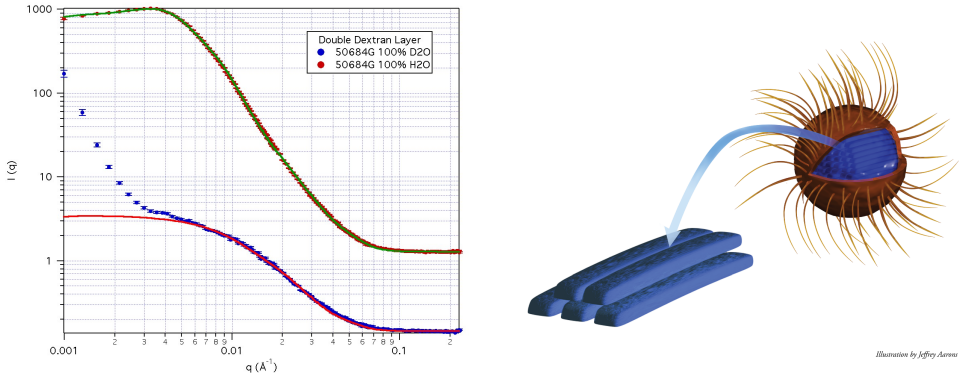

(a) (b)

Figure 1: (a) SANS results for nanoparticles in H_2O (red symbols) and D_2O (blue symbols); and (b) artists impression of the proposed core-shell structure

makes use of the fact that whilst the *nuclear* scattering had been removed by contrast matching, the *magnetic* scattering had not. The data fitted best with a description of the magnetic structure of the core consisting of parallelepipeds of magnetite packed together. This matched with X-ray diffraction data and information about the preparation of the particles.

However, in order to determine with certainty that the scattering from the nanoparticles in D_2O is indeed from the magnetic structure of the nanoparticle cores, we need a technique that can separate the nuclear and magnetic contributions to the scattering. Hence, we will employ polarized beam small angle neutron scattering to examine this system and determine the origin of the scattering observed in D_2O.

2 Why use SANS?

Generally, static light scattering and small angle X-ray scattering (SAXS) provide the same information about the sample as neutron scattering *i.e* measurement of macroscopic scattering cross-section $d\Sigma/d\Omega(q)$. The contrast in light scattering arises from the difference in the light's refractive index between the particle and water. The wavelength of light limits q < 0.002 Å^{-1} and thus the size range probe to $>\sim$3000Å. The contrast in X-ray scattering arises from the variation in electron density within the sample. However, this does not allow for good contrast between elements that are close in the periodic table and with many samples X-rays (particularly at synchrotron sources) can cause damage to the sample as a result of the large amount of energy imparted.

In the case of SANS the contrast arises from variations in the density and chemical composition within the sample. This allows for isotopic substitution to alter the scattering - a powerful technique known as "contrast variation". Additionally, neutrons are scattered by the magnetic moments of atoms within a material and so can determine both the chemical and magnetic structure of materials. Indeed, by using polarized neutrons (as you will learn here) it is possible to separate the two and determine them independently.

SANS is therefore an ideal probe for the structure of these magnetic nanoparticle systems since

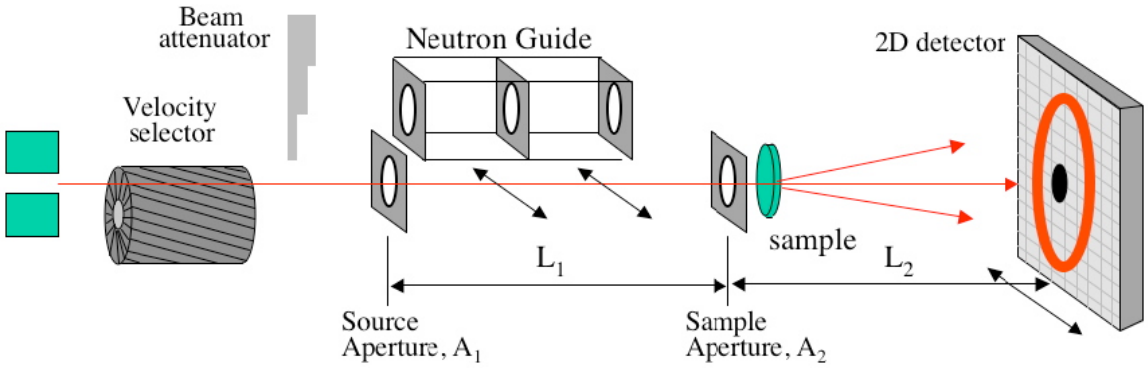

Figure 2: Schematic diagram of the components of the NCNR's 30-m SANS instruments.

we can measure on the necessary length scales, we can use contrast variation to examine both the magnetite core and the dextran shell, and we can examine the magnetic structure of the magnetite core.

3 Objectives of the Experiment

Obtain the nuclear and magnetic scattering cross sections By using a polarized neutron beam, ^{3}He analysis of the scattered neutrons and polarization correction data will be obtained that can then be processed to obtain the different components of the total scattering cross section.

Determine the magnetic structure of the nanoparticles The processed data will be analyzed by fitting model scattering functions to determine the details of the magnetic structure of the nanoparticles.

4 The SANS Instrument

Fundamentally, the SANS experiment consists of measuring the number of neutrons scattered per incoming neutron as a function of scattering angle. Since the size probed is inversely proportional to angle, to examine larger objects we need to measure scattering at smaller angles. In the case of a "pinhole" SANS instrument (such as the NG3 beamline at the NCNR) this is achieved by moving a 2 dimensional detector relative to the sample such that a detector element subtends a smaller angle the further the detector is from the sample.

Figure 2 shows a schematic of the 30 m NG3 SANS beamline at the NCNR without any of the polarized beam components.

In the case of an non-polarized beam experiment, the intensity of scattering on the detector after background correction in the SANS experiment is given by

$$I_{meas} = \phi A d T (\frac{d\Sigma}{d\Omega}) \Delta\Omega \varepsilon t \tag{1}$$

where

ϕ is the number of neutrons per second per unit area incident on the sample

A is the sample area

d is the sample thickness

T is the sample transmission

$\Delta\Omega$ is the solid angle over which scattered neutrons are accepted by the analyzer

ε is the detector efficiency

t is the counting time

The aim of a SANS experiment is to obtain the differential macroscopic scattering cross section $\frac{d\Sigma}{d\Omega}$ from I_{meas}. Matters are complicated when polarization of the incoming beam and polarization analysis of the scattered neutrons are included, but the fundamental aim remains. How we go about the process of extracting the cross section is described later, but first we need to decide how to prepare our samples for the measurement.

5 Planning the Experiment

Given the stated objectives of the experiment and knowledge of the instrument, how do we go about preparing for the experiment to maximize our chances of success? Here we discuss some of the issues that bear on this question.

5.1 Scattering Contrast

In order for there to be small-angle scattering, there must be scattering contrast between, in this case, the nanoparticle and the water. The scattering is proportional to the scattering contrast, $\Delta\rho$, *squared* where

$$\Delta\rho = \rho_{np} - \rho_{water} \tag{2}$$

and ρ_{np} and ρ_{water} are the *scattering length densities* (SLD) of the nanoparticle and the water, respectively. Recall that SLD is defined as

$$\rho = \frac{1}{V} \sum_{i}^{N} b_i \tag{3}$$

where V is the volume containing n atoms, and b_i is the (bound coherent) *scattering length* of the ith atom in the volume V. V is usually the molecular or molar volume for a homogenous phase in the system of interest.

Neutrons are scattered either through interaction with the nucleus (*nuclear scattering*) or through interaction between unpaired electrons (and hence the resultant magnetic moment) with the magnetic moment of the neutron (*magnetic scattering*). Hence a magnetic material such as magnetite will have both a *nuclear* scattering length density and a *magnetic* scattering length density and will display both a nuclear and magnetic contrast.

The SLDs for the phases in the present case, nanoparicle and water, can be calculated from the above formula, using a table of the scattering lengths (such as Sears,1992 [24]) for the elements, or can be calculated using the interactive SLD Calculator available at the NCNR's Web pages [25]. The SLDs for the components in this experiment are given below in Table 1.

Material	**Chemical Formula**	**Mass Density (g cm^{-3})**	**SLD$_n$ (Å^{-2})**	**SLD$_m$ (Å^{-2})**
Iron Oxide	Fe_3O_4	5.15	6.91×10^{-6}	1.46×10^{-6}
Dextran	$H(C_6H_{10}O_5)_nOH$	1.54	1.8×10^{-6}	0
Light Water	H_2O	1.0	-0.52×10^{-6}	0
Heavy Water	D_2O	1.0	6.32×10^{-6}	0

Table 1: The scattering length densities for Iron Oxide, dextran, heavy and light water

5.2 Sample Thickness

Given the calculated sample contrast, how thick should the sample be? Recall that the scattered intensity is proportional to the product of the sample thickness, d_s and the sample transmission, T. It can be shown that the transmission, which is the ratio of the transmitted beam intensity to the incident beam intensity, is given by

$$T = e^{-\Sigma_t d_s} \tag{4}$$

where $\Sigma_t = \Sigma_c + \Sigma_i + \Sigma_a$, i.e. the sum of the coherent, incoherent and absorption macroscopic cross sections. The absorption cross section, Σ_a, can be accurately calculated from tabulated absorption cross sections of the elements (and isotopes) if the mass density and chemical composition of the sample are known. The incoherent cross section, Σ_i, can be *estimated* from the cross section tables for the elements as well, but not as accurately as it depends on atomic motions and is therefore temperature dependent. The coherent cross section, Σ_c, can also only be estimated since it depends on the details of both the structure and the correlated motions of the atoms in the sample. This should be no surprise as Σ_c as a function of angle is the quantity we are aiming to measure!

The scattered intensity is proportional to d_sT and hence

$$I_{meas} \propto d_s e^{-\Sigma_t d_s} \tag{5}$$

which has a maximum at $d_s = 1/\Sigma_t$ which implies an optimum transmission, $T_{opt} = 1/e = 0.37$. The sample thickness at which this occurs is known as the "1/e length".

The NCNR web based SLD calculator provides estimates of Σ_i and Σ_a and gives an estimate of the 1/e length as well as calculating the SLD.

In this experiment, the optimum sample thickness has been determined to be 1mm.

5.3 Magnetic Scattering

Small-angle neutron scattering (SANS) is ideal for obtaining both nuclear and magnetic structure, even small magnetic moments, with sub-nanometer resolution (Fig. 3).

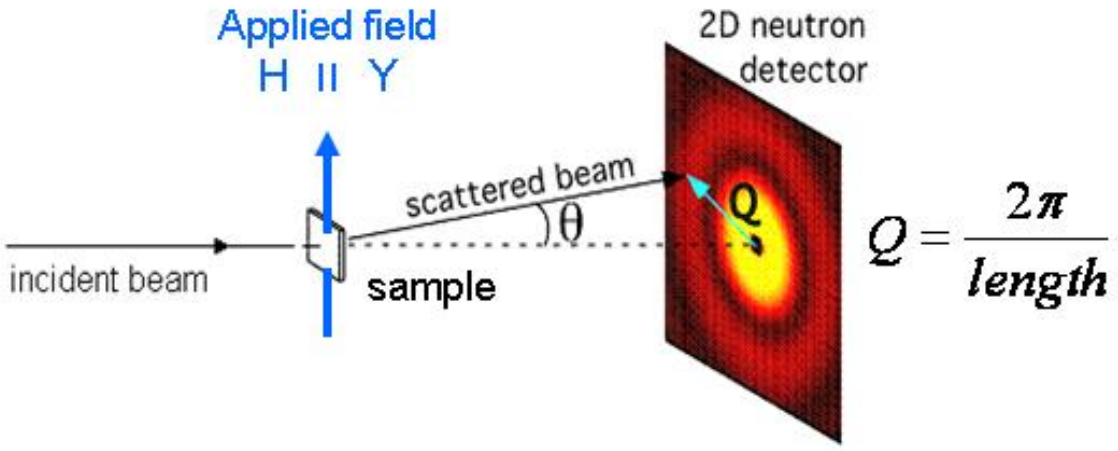

Figure 3: General (unpolarized) SANS set-up. The rule is that scattering can only be observed from the component of magnetic moments oriented *perpendicular* to $\vec{Q}$.

Selection rules dictate that only the component of the magnetic moment that is perpendicular to the scattering wave vector, $\vec{Q}$, can participate in scattering. The measured scattering intensity, I, is proportional to the squared sum of the spatial nuclear (N^2) and magnetic (M^2) Fourier transforms defined as

$$N, M_J(Q) = \sum_K \rho_{N,M_J}(K) e^{i\vec{Q}\cdot\vec{R}_K} \tag{6}$$

where J is any Cartesian coordinate, $\rho_{N,M}$ is the nuclear or magnetic scattering length density, and $\vec{R}_K$ is the relative position of the Kth scatterer.

As example, consider the case of 9 nm, spherical Fe_3O_4 nanoparticles, closed packed with a nearest neighbor distance of 7.8 nm. Application of a field greater than a Tesla saturates the sample and causes all the moments in the sample to align parallel to the field direction. The close packed structure produces a nearest-neighbor nuclear and magnetic Bragg scattering peak 0.080 $\mathring{A}^{-1}$ (Fig. 4). Sector slices about the X-axis (nuclear + magnetic scattering) versus the Y-axis (nuclear only), shown on the right hand side of Fig. 4, are remarkably similar. This can be understood by re-examining the relative nuclear and magnetic scattering length densities, ρ_N=6.97 x 10^{-6} $\mathring{A}^{-2}$ and ρ_M=1.46 x 10^{-6} $\mathring{A}^{-2}$, respectively. Even if fully saturated, magnetic scattering is produced, at

most $\left(\frac{\rho_M}{\rho_N}\right)^2$ is only equal to 4 %. Clearly, we need a better approach for measuring small magnetic signals.

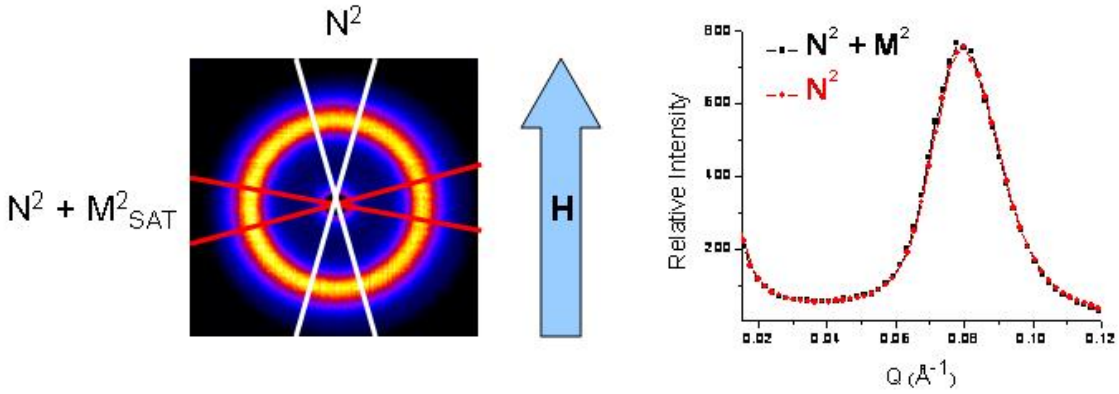

Figure 4: Unpolarized scattering shows only a small magnetic component along the horizontal with a saturating field applied along the vertical.

5.3.1 Polarization

Once the neutron spin polarization axis has been defined by the presence of a magnetic field (even a small field), the beam can be polarized (i.e. one spin state is preferentially selected over the other) by scattering from an FeSi supermirror (Fig. 5).

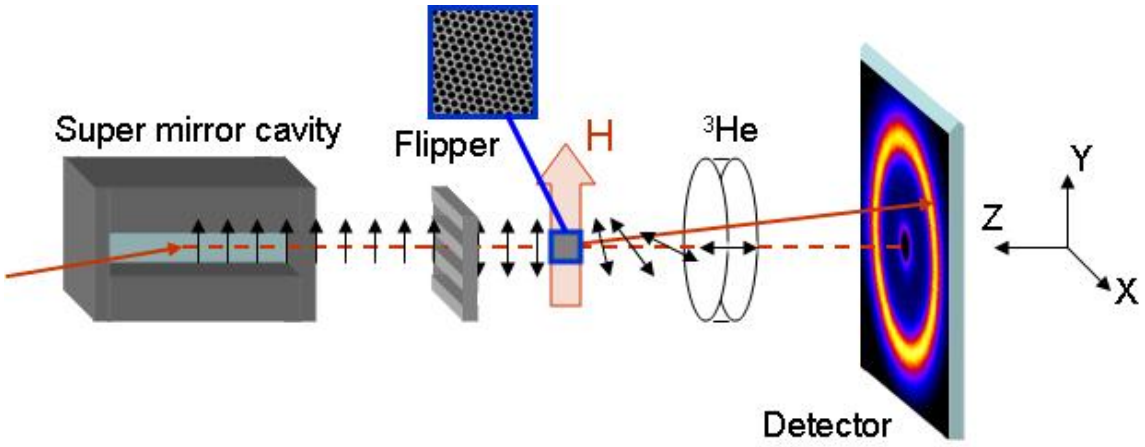

Figure 5: Polarized SANS set-up includes a polarizing FeSi supermirror, an electromagnetic coil that can reverse the neutron spin direction at will, a variable magnetic field at the sample position, and a ^{3}He analyzing cell capable of sampling a divergent, scattered beam.

The supermirror is a specially made diffraction grating that looks different to neutrons aligned parallel and antiparallel to the applied field, thus scattering them at different angles. We send the ↑ neutrons down the beamline, but can reverse their direction at will using an electromagnetic

flipper coil. An analyzing glass cell filled with polarized ^{3}He gas preferentially allows neutrons with spins aligned with the ^{3}He atoms to pass through, while absorbing neutrons of the other spin state [26]. The ^{3}He orientation, too, can be reversed at will with a nuclear magnetic resonance (NMR) pulse of an appropriate frequency. As discussed in detail later, the ^{3}He polarization is time dependent. For any polarizing/analyzing apparatus, the degree of polarization (P) is defined as the difference between the $\uparrow$ and $\downarrow$ neutrons after passing thus a polarizing device, divided by the total number of incoming neutrons $(\uparrow + \downarrow)$ as

$$P \equiv \left| \frac{I_\uparrow - I_\downarrow}{I_\uparrow + I_\downarrow} \right|. \tag{7}$$

The utility of adding polarization for measuring M^2 is immediately obvious in Fig. 6 (compare to Fig. 4). Sector slices about the X-axis and Y-axis from $\uparrow$ *to* $\uparrow$ and $\downarrow$ *to* $\downarrow$ scattering now contain easily observed $\pm$ NM cross-terms (Fig. 6).

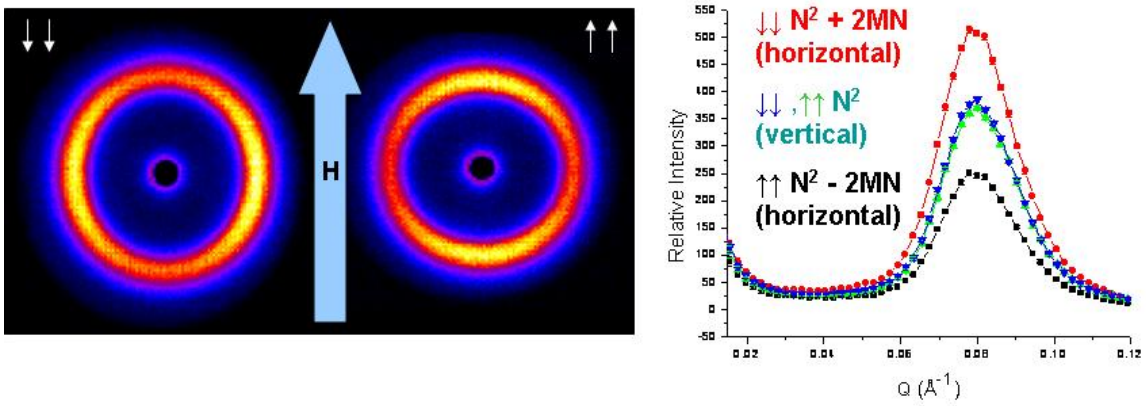

Figure 6: Polarization analysis yields an obvious magnetic scattering component, compared to the unpolarized case in Fig. 4.

5.3.2 Spin Selection Rules

Polarization analyzed SANS can uniquely separate the nuclear scattering (N^2) from magnetic scattering of moments parallel to the applied field ($M_Y^2 = M_{PARL}^2$) and those perpendicular to the applied field ($M_X^2 + M_Z^2 = 2M_{PERP}^2$) for any field ≥ 0.001 Tesla. Area-normalized sector slices of $\pm\ 10^o$ are taken about specific θ angles of interest in order to extract angular information, where θ is the angle between the X axis (horizontal midline of the detector) and the projection of $\vec{Q}$ onto the X-Y detector plane. The complete, angle-dependent polarization selection rules (Appendix A) simplify at several key angles as follows:

$$N^2(Q) = \frac{1}{2}(I^{\uparrow\uparrow}_{\theta=90^o} + I^{\downarrow\downarrow}_{\theta=90^o}) \tag{8}$$

$$M^2_{PARL}(Q) = \frac{(I^{\downarrow\downarrow}_{\theta=0^o} - I^{\uparrow\uparrow}_{\theta=0^o})^2}{16N^2} \tag{9}$$

$$M^2_{PERP}(Q) = \frac{1}{6}(I^{\uparrow\downarrow}_{\theta=0^o,90^o} + I^{\downarrow\uparrow}_{\theta=0^o,90^o}) \tag{10}$$

$$M^2_{PARL}(Q) = (I^{\uparrow\downarrow}_{\theta=45^o,135^o} + I^{\downarrow\uparrow}_{\theta=45^o,135^o}) - 5M^2_{PERP} \tag{11}$$

M^2_{PARL} profiles extracted using Eqn. 9 or 11 should be equivalent. The main points to remember are that $\uparrow$ *to* $\uparrow$ and $\downarrow$ *to* $\downarrow$ (or non spin-flip scattering, NSF) contains information about N^2 and M^2_{PARL}, while $\uparrow$ *to* $\downarrow$ and $\downarrow$ *to* $\uparrow$ (or spin-flip scattering, SF) contains only magnetic scattering.

By taking the appropriate sector slices and from the 2D data sets and processing them in conjunction with Eqns. 8-11, we can resolve N^2, M^2_X, M^2_Y, and M^2_Z – that is we can extract 3D magnetic scattering information independent of the typically dominant nuclear scattering, but only after correcting the raw data for the efficiencies of the polarizing elements (described below).

6 Collecting Data

6.1 Configuring the instrument

We must decide how to configure the SANS instrument to measure the appropriate Q range efficiently. Here again we can use a computational tool, called SASCALC, as a guide. A schematic of the NCNR's 30 m SANS instrument is shown in Fig. 2, and the instrument configuration parameters, and their allowed range for the NG-3 30 m SANS instrument, are listed in Table 2.

Variable	**Allowed Range**
Source:	neutron guide (NG3), 6 x 6 cm2
Monochromator:	mechanical velocity selector with variable speed
Wavelength Range:	5 to 20 Å
Wavelength Resolution (FWHM):	10 to 30% wavelength spread
Source-to-Sample Distance:	3.5 to 15 m in 1.5 m steps via insertion of neutron guide segments
Sample-to-Detector Distance:	1.3 to 13.2 m continuously variable
Detector Offset:	0 – 25 cm (translation perpendicular to beam to extend the q-range covered at a given SDD)
Beam stop diameter:	2.54, 5.08, 7.62 or 10.16 cm
Beam Attenuator:	10 thicknesses to reduce beam intensity
Collimation:	circular pinhole collimation
Sample Size:	0.5 to 2.5 cm diameter
Q range:	0.015 to 6 nm-1
Size Regime:	1 to 600 nm
Detector:	64 x 64 cm2 He-3 position-sensitive proportional counter (0.5 x 0.5 cm2 resolution)
Unique feature:	neutron polarization

Table 2: Instrument configuration parameters and their range of allowed values for the NG-3 30-m SANS instrument. [27]

In the case of a polarized beam experiment, our choices are limited by the fact that the supermirror polarizer is at a specific location in the neutron guide path (at the position of the 7th guide element) and so our source-to-sample distance is fixed. We have a choice of two ^{3}He cells with differing characteristic wavelengths - 5Å and 7.5Å. Thus our accessible Q range is defined by the combination of sample-to-detector distance and wavelength.

Given these restrictions, for this experiment it has been determined that the most appropriate instrument configuration uses 7.5Å neutrons, 7 neutron guides, a 1" source aperture, a 0.5" sample aperture and a sample-to-detector distance of 4.55 meters. This yields a Q range of 0.006 Å^{-1} to 0.08 Å^{-1}.

6.2 What measurements to make

In addition to measuring the scattering from the sample a number of other measurements need to be made.

6.2.1 Background Corrections

To correct for instrument "background" measurement of scattering without the sample is needed. Counts recorded on the detector can come from three sources: 1) neutrons scattered by the sample itself; 2) neutrons scattering from something other than the sample, *but which pass through the sample*; and 3) everything else, including neutrons that reach the detector *without passing through the sample* (stray neutrons or so-called room background) and electronic noise in the detector itself.

In order to separate these contributions we need to make three separate measurements:

1. Scattering measured with the sample in place (which contains contributions from all three sources listed above), $\mathbf{I_{sam}}$
2. Scattering measured with the empty sample holder in place (which contains contributions from sources 2 and 3 above), $\mathbf{I_{emp}}$
3. Counts measured with a complete absorber at the sample position (which contains only the contribution from source 3 above), $\mathbf{I_{bgd}}$

6.2.2 Polarization Efficiencies

The polarizing elements (supermirror, flipper, and ^{3}He filter) aren't 100 % efficient, and so leakage of neutrons with an unwanted spin state must be accounted for. Using the four experimental scattering cross-sections that you will collect ($S_{\uparrow\uparrow}$, $S_{\downarrow\uparrow}$, $S_{\downarrow\downarrow}$, and $S_{\uparrow\downarrow}$) and your experimentally measured the polarization efficiencies for each polarizing element,the program Pol-Corr can automatically do this correction for you (details in Appendix B). To determine the polarization of the ^{3}He cell (P_{Cell}) at any given time we use the following equations (details in Appendix F). T stands for a transmission measurements, while S means a scattering measurements. Taking a blocked beam measurement allows us to remove electronic detector noise and the contribution from those neutrons that scatter around the sample area. An unpolarized beam is produced by simply removing the

upstream supermirror. Note that the polarizing power of the ^{3}He cell (P_{Cell}) is not the same as the polarization state of its constituent ^{3}He atoms ($\wp_{^3He\ atoms}$).

$$P_{Cell} = tanh(\mu\wp_{^3He\ atoms}) \tag{12}$$

$$\mu\wp_{^3He\ atoms} = acosh\left(\frac{T_{cell,\ unpolarized\ beam} - T_{blocked,\ unpolarized\ beam}}{[T_{empty,\ unpolarized\ beam} - T_{blocked,\ unpolarized\ beam}]\,T_E e^{-\mu}}\right). \tag{13}$$

T_E, the transmission of an unfilled cell, and neutron attenuation length or opacity, μ are known with high precision for each ^{3}He cell. They can be verified, however, by measuring by the transmission of a depolarized ^{3}He cell (Appendix G).

Now that we know the polarization of our analyzer, we can determine the polarization of the supermirror (P_{SM}) and flipper (P_F) using the following equations where $T_{blocked}$ means a blocked *polarized* beam (see Appendix E for details),

$$P_{SM} = \frac{\frac{T_{\uparrow\uparrow} - T_{blocked}}{T_{\uparrow\downarrow} - T_{blocked}} - 1}{P_{Cell}(1 + \frac{T_{\uparrow\uparrow} - T_{blocked}}{T_{\uparrow\downarrow} - T_{blocked}})} \tag{14}$$

$$P_F = \frac{\frac{T_{\downarrow\downarrow} - T_{blocked}}{T_{\downarrow\uparrow} - T_{blocked}} - 1}{P_{SM}P_{Cell}(1 + \frac{T_{\downarrow\downarrow} - T_{blocked}}{T_{\downarrow\uparrow} - T_{blocked}})}. \tag{15}$$

Typical values of P_{SM} and P_F are 0.90 to 0.95 and 0.96, respectively. If the sample has any depolarizing effect on the beam due to the presence of its own magnetic domains (e.g. distinct internal magnetic regions containing a net magnetic moment), this will fold into the measurement of P_{SM} (discussed in Appendix C).

6.2.3 Time dependence of the ^{3}He

The ^{3}He cell is polarized away from the neutron beamline using a high-powdered laser system, and its polarization slowly decays with a lifetime (Γ) of approximately 70 to 150 hours, depending on the stray field conditions. Both Γ and time (t) are measured in hours, and the time of collection for each data set can be computed from a time stamp embedded in its associated header.

$$\mu\wp_{3He}(t_n) = \mu\wp_{3He}(t_0)e^{\frac{t_0 - t_n}{\Gamma}}. \tag{16}$$

There are several ways to measure Γ (Appendix F), but we shall focus only on the simplest experimentally measured approach here. Using Eqn. 13 we can measure $\mu\wp_{3He}$ at any chosen time intervals simply be removing the supermirror, and we will measure $\mu\wp_{3He}(t_0)$ at the start of the experiment (defined as time zero). Thus, we can fit the Γ using the following relation for a series of $\mu\wp_{3He}(t_n)$s measured during the course of the experiment,

$$\Gamma = (t_0 - t_n)\ ln(\frac{\mu\wp_{3He}(t_0)}{\mu\wp_{3He}(t_n)}). \tag{17}$$

Or if preferred, one can also fit Γ as an exponential decay term from the plot of $\mu\wp_{3He}$ versus time (Eqn. 16).

6.3 Experimental Measurements

The sample will be mounted and aligned in the beam when you arrive and the wavelength will be set to 7.5 $\AA$. Your experiment will be performed in a very low magnetic field of 0.0015 Tesla (15 Gauss). This defines a polarization axis for the neutrons so that you can do the polarization analysis, while negligibly affecting the sample's magnetic configuration. You'll be able to verify that a small polarizing field exists all the way between the supermirror and flipper to the ^{3}He cell using a Gaussmeter. You should be also to quickly see that the non spin-flip scattering (containing nuclear scattering) is much more intense that spin-flip scattering (magnetic only).

The first quantitative measurements will involve taking (A) an unpolarized blocked-beam transmission, (B) an empty, unpolarized transmission, and (C) an unpolarized transmission with the ^3He cell moved into the beam. The transmissions will be taken at a detector distance of 13 m in order to cover as many detector pixels as possible (this requires fewer protective attenuators than a closer detector distance, and, thus, yields better counting statistics). Using these measurements and Eqn. 13 you will calculate the cell opacity (μ) multiplied by the polarization of the ^{3}He cell ($\wp_{^3He}(t_0)$) at the start of your experiment.

Next, you will translate the supermirror into the beam to create a polarized beam. First, take a polarized blocked beam transmission. By taking a combination of flipper on and off, and reversing or *flipping* the orientation of the ^{3}He cell with a NMR pulse, you will collect all four transmission cross-sections ($T_{\uparrow\uparrow}$, $T_{\downarrow\uparrow}$, $T_{\downarrow\downarrow}$, and $T_{\uparrow\downarrow}$). Using Eqns. 14 and 15 you will determine the polarizations of the supermirror and flipper, respectively.

Having made the initial measurements for quantifying the efficiencies of the polarizer and analyzer, the sample, empty cell and blocked beam measurements can now be made. During the night you will set-up long scattering scans for all four cross-sections. The stronger NSF scattering files will be counted for 1.5 hours each, while the weaker spin-flip files will be counted for 3 hours each. You will also set-up an empty sample holder to get background (since this produces no genuine magnetic scattering, only one non spin-flip file and one spin-flip file are required). A blocked beam measurement will also be made. You will also periodically take unpolarized transmissions at 13 m in order to determine Γ and the resulting polarization of the ^{3}He cell as a function of time.

7 Data Reduction and Analysis

After collecting data overnight, the first task will be to correct the scattering data files for instrumental geometry effects, sample transmission and detector efficiency.

Having performed initial corrections on your scattering data you will fit Γ using Eqns. 16 or 17 in combination with the measured $\wp_{^3He}(t_n)$s (Eqn. 13). Using this value of Γ, plus your measured values of P_{SM}, P_F, μT_E, and $\wp_{^3He}(t_0)$ from the previous day, you will polarization correct your scattering data files and your background scattering files using the program Pol-Corr (will be shown to you by your instructors).

You should be able to see definite, angular dependencies corresponding to Eqns. 8-11 that arise from the magnetic contributions. By taking sector slices about appropriate axes and applying Eqns. 8-11, you will be able to extract N^2, M^2_{PARL}, M^2_{PERP}.

The nuclear and magnetic scattering cross sections will then be analyzed to determine the magnetic structure of the nanoparticles compared to the nuclear structure.

Appendices

These appendices provide all of the calculation details and assumptions that have gone into the polarization corrections for users who are curious. The justifications for the measurement procedures are also provided here. In practice, knowledge of these details are not necessary when performing a standard polarized beam experiment. However, they are included for completeness and for reference.

In all that follows subscripts denote the orientation of the majority of neutron spins that make it the detector (i.e. $\uparrow\uparrow$ means that the supermirror is in, the flipper is off, and the ^{3}He atoms are oriented $\uparrow$). Superscripts, where used, indicate the actual number, not the measured number with some polarization leakage included, of spins that traverse through with a specific element or combination of elements. Along the same lines, σ indicates the true cross-section, compared to the measured intensity, I (specifically measured as transmission, T, or scattering, S), which includes leakage from other spin-states prior to polarization correction.

Appendix A Vectorial Spin Selection Rules

Vectorial analysis of the spin-dependent neutron scattering is typically described in terms of the Halpern-Johnson vector which encompasses the fact that only magnetic moments perpendicular to $\overrightarrow{Q}$ participate in scattering, while the nuclear scattering only appears in non spin-flip scattering. Here we use a modified version of the Halpern-Johnson vector (Υ) expressed in terms of angle as

$$\Upsilon_J(Q) = \sum_{L=X,Y,Z} M_L(cos(\phi_{L,J}) - cos(\phi_{\mathbf{Q},J})cos(\phi_{\mathbf{Q},L})) \tag{18}$$

where ϕ denotes the angle between subscripted variables. J refers to the Υ direction, while L is used to indicate a sum over three cartesian coordinates. If the A axis defines the applied field direction, with $\hat{B} \times \hat{C} = \hat{A}$ then [28]

$$I^{\downarrow\downarrow,\uparrow\uparrow}(Q) = |N \pm \Upsilon_A|^2 \tag{19}$$

$$I^{\uparrow\downarrow,\downarrow\uparrow}(Q) = |\Upsilon_B \mp i\Upsilon_C|^2. \tag{20}$$

With the field direction set to $\hat{X}$, the detector set in the $X-Y$ plane, and $\hat{Z}$ defining the beam direction, this becomes

$$\begin{aligned} I^{\downarrow\downarrow,\uparrow\uparrow}(Q) = N^2 + M_X^2 sin^4(\theta) + M_Y^2 cos^2(\theta) sin^2(\theta) \\ -2M_X M_Y sin^3(\theta)cos(\theta) \pm 2NM_X sin^2(\theta) \mp 2NM_Y cos(\theta)sin(\theta) \end{aligned} \tag{21}$$

$$I^{\uparrow\downarrow,\downarrow\uparrow}(Q) = M_Z^2 + M_Y^2 cos^4(\theta) + M_X^2 sin^2(\theta)cos^2(\theta) - 2M_X M_Y sin(\theta)cos^3(\theta). \tag{22}$$

These equations simplify at $\theta = 0^o, 45^o, 90^o$, and 135^o [29]. If the field is instead applied along $\hat{Y}$, the result is to rotate the θ angle by 90^o, and this is the basis for Eqs. 3-6 utilized in the main text for data processing. In fact the polarized scattering behavior for any applied field direction, such as $\hat{Z}$ for example, can be derived using Eqns. 1-3.

Appendix B Mechanics of Polarization Efficiency Corrections

Let us consider the polarized beamline set-up as three parts: a front-end (F) comprised of a supermirror and a flipper, the middle area containing the sample, and a back-end (B) occupied by the ^{3}He analyzer. What we want is to extract the sample scattering cross-sections, σ, from the experimentally measured intensities, I. The simplest approach is to use matrix form, which will later be inverted to yield the desired σs. Here F and B refer to the actual fraction of neutrons with a given spin (denoted in superscript) divided by the total number of neutrons that pass through the configuration of polarizing elements (indicated by subscript). This definition for F and B is commonly referred to as an efficiency, ε.

$$\underbrace{\begin{bmatrix} F^{\uparrow}_{(\uparrow)}B^{\uparrow}_{(\uparrow)} & F^{\downarrow}_{(\uparrow)}B^{\uparrow}_{(\uparrow)} & F^{\downarrow}_{(\uparrow)}B^{\downarrow}_{(\uparrow)} & F^{\uparrow}_{(\uparrow)}B^{\downarrow}_{(\uparrow)} \\ F^{\uparrow}_{(\downarrow)}B^{\uparrow}_{(\uparrow)} & F^{\downarrow}_{(\downarrow)}B^{\uparrow}_{(\uparrow)} & F^{\downarrow}_{(\downarrow)}B^{\downarrow}_{(\uparrow)} & F^{\uparrow}_{(\downarrow)}B^{\downarrow}_{(\uparrow)} \\ F^{\uparrow}_{(\downarrow)}B^{\uparrow}_{(\downarrow)} & F^{\downarrow}_{(\downarrow)}B^{\uparrow}_{(\downarrow)} & F^{\downarrow}_{(\downarrow)}B^{\downarrow}_{(\downarrow)} & F^{\uparrow}_{(\downarrow)}B^{\downarrow}_{(\downarrow)} \\ F^{\uparrow}_{(\uparrow)}B^{\uparrow}_{(\downarrow)} & F^{\downarrow}_{(\uparrow)}B^{\uparrow}_{(\downarrow)} & F^{\downarrow}_{(\uparrow)}B^{\downarrow}_{(\downarrow)} & F^{\uparrow}_{(\uparrow)}B^{\downarrow}_{(\downarrow)} \end{bmatrix}}_{Measured\ Polarization\ Efficiencies} \underbrace{\begin{bmatrix} \sigma^{\uparrow\uparrow} \\ \sigma^{\downarrow\uparrow} \\ \sigma^{\downarrow\downarrow} \\ \sigma^{\uparrow\downarrow} \end{bmatrix}}_{Cross-Sections} = \underbrace{\begin{bmatrix} I_{(\uparrow\uparrow)} \\ I_{(\downarrow\uparrow)} \\ I_{(\downarrow\downarrow)} \\ I_{(\uparrow\downarrow)} \end{bmatrix}}_{Experimental\ Data} \tag{23}$$

Recall, that polarization for an element with $\uparrow$ being the majority state can be written as

$$P = \frac{I^{\uparrow} - I^{\downarrow}}{I^{\uparrow} + I^{\downarrow}}. \tag{24}$$

And efficiencies for $\uparrow$ and $\downarrow$ neutrons ($\varepsilon^{\uparrow}$ and $\varepsilon^{\downarrow}$) can be written in terms of P as

$$\varepsilon^{\uparrow} \equiv \frac{I^{\uparrow}}{I^{\uparrow} + I^{\downarrow}} = \frac{1+P}{2} \tag{25}$$

$$\varepsilon^{\downarrow} \equiv \frac{I^{\downarrow}}{I^{\uparrow} + I^{\downarrow}} = \frac{1-P}{2} \tag{26}$$

Thus, we can relate the Fs and Bs to the experimentally measurable polarization values of the supermirror, flipper, and ^{3}He cell using

$$F^{\uparrow}_{(\uparrow)} = \left(\frac{1+P_{SM}}{2}\right);\ F^{\downarrow}_{(\uparrow)} = \left(\frac{1-P_{SM}}{2}\right);\ F^{\downarrow}_{(\downarrow)} = \left(\frac{1+P_F P_{SM}}{2}\right);\ F^{\uparrow}_{(\downarrow)} = \left(\frac{1-P_F P_{SM}}{2}\right) \tag{27}$$

and

$$B^{\uparrow}_{(\uparrow)} = B^{\downarrow}_{(\downarrow)} = \left(\frac{1+P_{Cell}}{2}\right);\ B^{\uparrow}_{(\downarrow)} = B^{\downarrow}_{(\uparrow)} = \left(\frac{1-P_{Cell}}{2}\right). \tag{28}$$

Note that P_{Cell} is time dependent (Appendix F). With the I's measured, and the Fs and Bs determined from experiment, σs are easily determined by matrix inversion. This is facilitated by use of the program Pol-Corr where the time that each data set was acquired is automatically read from its header file. Multiple files for a given I measurement may be added together (after normalization by the monitor counter) for increased statistics, while the corresponding FBs are computed as linear combination of each file's FB.

Appendix C Sample Depolarization

If you have a sample that contains multiple internal magnetic regions, or domains, this can abruptly change the magnetic field the neutron experiences as it passes through. This magnetic abruptness can flip some of the neutron spins without the action of sample scattering, in a process known as beam *depolarization*. While this is not a desirable state, it can be readily measured and accounted for. Additionally, thin samples are less depolarizing. Let us denote the [ideally small] fraction of neutrons that the sample (or quickly-varying stray magnetic field) inadvertently flips independent of any sample scattering as χ_D, so that

$$F^{\uparrow}_{(\uparrow)} = \left(\frac{1+P_{SM}}{2}\right)(1-\chi_D) + \left(\frac{1-P_{SM}}{2}\right)(\chi_D) \tag{29}$$

$$F^{\downarrow}_{(\uparrow)} = \left(\frac{1-P_{SM}}{2}\right)(1-\chi_D) + \left(\frac{1+P_{SM}}{2}\right)(\chi_D) \tag{30}$$

$$F^{\downarrow}_{(\downarrow)} = \left(\frac{1+P_F P_{SM}}{2}\right)(1-\chi_D) + \left(\frac{1-P_F P_{SM}}{2}\right)(\chi_D) \tag{31}$$

$$F^{\uparrow}_{(\downarrow)} = \left(\frac{1-P_F P_{SM}}{2}\right)(1-\chi_D) + \left(\frac{1+P_F P_{SM}}{2}\right)(\chi_D) \tag{32}$$

If P_{SM} is replaced by $P'_{SM} = P_{SM}(1-2\chi_D)$, then Eqns. 29-32 can be written exactly in the form of Eqn. 27. This proves that the sample depolarization is directly coupled with the measurement of P_{SM}. Practically, this means that if a sample condition is changed in a manner that might alter χ_D, then a new P_{SM} should always be measured.

Appendix D ^{3}He Polarization [26]

Let us refer to the transmission of the neutron with spins parallel to the ^{3}He cell as the majority state, and those antiparallel as the minority state,

$$T_{^3He}^{Majority,Minority} = \frac{1}{2} T_E e^{-\mu(1\mp\wp_{^3He})}. \tag{33}$$

T_E, the transmission of an unfilled ^{3}He cell, and μ, the attenuation length or opacity of the ^{3}He cell, are typically well quantified for each cell used. (However, $T_E e^{-\mu}$ can be measured directly using a depolarized ^{3}He cell, as described in Appendix G, as a double check. This is typically performed at the the end of an experiment since it takes a while to re-polarize a fully depolarized cell.) If we apply an *unpolarized beam* to our *polarized* ^{3}He cell, then the number of parallel and antiparallel neutrons should be equivalent, and we can write the total transmission through the ^{3}He cell as

$$T_{3He}^{Total} = T_{^3He}^{Majority} + T_{^3He}^{Minority} = T_E(e^{-\mu(1-\wp_{^3He})} + e^{-\mu(1+\wp_{^3He})}) = T_E e^{-\mu} cosh(\mu\wp_{^3He}). \tag{34}$$

$$\mu\wp_{^3He} = acosh\left(\frac{T_{3He}^{Total}}{T_E e^{-\mu}}\right) \tag{35}$$

The polarization of the cell can be evaluated, using the quantity experimentally measured in Eqn. 35, as

$$P_{Cell} \equiv \left|\frac{T_{^3He}^{Majority} - T_{^3He}^{Minority}}{T_{^3He}^{Majority} + T_{^3He}^{Minority}}\right| = \frac{T_E e^{-\mu} sinh(\mu\wp_{^3He})}{T_E e^{-\mu} cosh(\mu\wp_{^3He})} = tanh(\mu\wp_{^3He}) \tag{36}$$

Appendix E Details of Supermirror and Flipper Polarizations

To solve for the supermirror and flipper efficiencies we must either remove the sample or make the assumption that negligible sample scattering contributes to the experimental transmissions. (Note that in order to measure the sample depolarization, coupled into P_{SM} as discussed in Appendix C, the sample must remain in the beam.) Without sample scattering, we know that spin-flip scattering ceases ($\sigma^{\uparrow\downarrow} = \sigma^{\uparrow\downarrow} = 0$) and non spin-flip scattering of either neutron spin direction are equivalent ($\sigma^{\uparrow\uparrow} = \sigma^{\downarrow\downarrow} \equiv \sigma^{Majority}$). Coupled with Eqns. 23 and 27-28, this produces for the flipper off states,

$$I^{\uparrow\uparrow} = \sigma^{Majority}\left[\left(\frac{1+P_{SM}}{2}\right)\left(\frac{1+P_{Cell}}{2}\right)+\left(\frac{1-P_{SM}}{2}\right)\left(\frac{1-P_{Cell}}{2}\right)\right] \tag{37}$$

$$I^{\uparrow\downarrow} = \sigma^{Majority}\left[\left(\frac{1+P_{SM}}{2}\right)\left(\frac{1-P_{Cell}}{2}\right)+\left(\frac{1-P_{SM}}{2}\right)\left(\frac{1+P_{Cell}}{2}\right)\right] \tag{38}$$

Dividing Eqn. 37 by Eqn. 38 and rearranging yields

$$P_{SM} = \frac{\frac{I_{\uparrow\uparrow}}{I_{\uparrow\downarrow}}-1}{\frac{I_{\uparrow\uparrow}}{I_{\uparrow\downarrow}}+1}\left(\frac{1}{P_{Cell}}\right) \tag{39}$$

Turning the flipper on similarly produces,

$$I^{\downarrow\downarrow} = \sigma^{Majority}\left[\left(\frac{1+P_{SM}P_F}{2}\right)\left(\frac{1+P_{Cell}}{2}\right)+\left(\frac{1-P_{SM}P_F}{2}\right)\left(\frac{1-P_{Cell}}{2}\right)\right] \tag{40}$$

$$I^{\downarrow\uparrow} = \sigma^{Majority}\left[\left(\frac{1+P_{SM}P_F}{2}\right)\left(\frac{1-P_{Cell}}{2}\right)+\left(\frac{1-P_{SM}P_F}{2}\right)\left(\frac{1+P_{Cell}}{2}\right)\right] \tag{41}$$

$$P_F = \frac{\frac{I_{\downarrow\downarrow}}{I_{\downarrow\uparrow}}-1}{\frac{I_{\downarrow\downarrow}}{I_{\downarrow\uparrow}}+1}\left(\frac{1}{P_{Cell}P_{SM}}\right) \tag{42}$$

As noted previously, P_{SM} is a measurement of the supermirror polarizations coupled with any sample depolarization. It is also important to remember that P_{Cell} varies as a function of time (Appendix F). Thus, the simplest option involves measuring P_{Cell} just prior to the transmission measurements that will be used to determine P_{SM} and P_F. This approach works because the cell lifetime is typically 70 to 150 hours at the SANS beamlines, dependent upon the stray magnetic fields it encounters.

Appendix F Time Dependence of the ^{3}He Cell

The ^{3}He cell [26] is polarized away from the neutron beamline using a high-powdered laser system, and its polarization slowly decays with a lifetime (Γ). Mathematically, this is described as

$$\wp_{3He}(t_n) = \wp_{3He}(t_o)e^{-(t_n - t_o)/\Gamma} \tag{43}$$

where t_n is any given time after the start of the experiment, t_0. Γ and t_n are usually expressed in hours. There are several approached that may be used to measure Γ, and, thus, calculate the polarization of the ^{3}He cell at any time that a data file was collected for processing in Pol-Corr.

F.1 Method A: Nuclear Magnetic Resonance

In many cases (such as when the ^{3}He cell can be located far enough away from stray magnetic field) nuclear magnetic resonance (NMR) is employed by the ^{3}He team to measure the decay of the ^{3}He atoms during the entire course of the experiment. In this case, only a single measure of $\wp_{^3He}(t_0)$ is needed to peg the absolute value of the polarization decay curve, and the uncertainty on Γ is quite low. However, when constant NMR measurement isn't applicable, there are two additional options to consider.

F.2 Method B: Measuring ^{3}He Polarization Using an Unpolarized Beam

If we can regularly remove the sample from the beam or if we can safely assume that the sample does *not polarize* the beam, then we can use Eqn. 35 to calculate a series the $\mu\wp_{^3He}$ during the course of an experiment. By plotting $\mu\wp_{^3He}$ (or, if preferred, $\wp_{^3He}$ for a known μ) as a function of time, Γ can be readily fit as an exponential decay constant Eqn. 43.

Even for cases in which the sample cannot be removed (for example when a fixed position cryostat is used), this approach should be valid unless the sample (in a highly unlikely scenario) happens to preferentially scatter one spin orientation over the other, such as a specifically engineered supermirror does at low incident angles. Conversely, the more common condition of sample depolarization is not in fact a problem because the original beam is already in an unpolarized state.

F.3 Method C: Measuring Flipping Ratios with a Polarized Beam

If we assume that negligible sample scattering goes into the measured transmissions, then from Eqn. 23 measurement of flipper on and off for a ^{3}He cell in the $\uparrow$ state yields,

$$T^{Expt}_{(\uparrow\uparrow)} = \sigma^{NSF}[(\frac{1+P_{SM}}{2})(\frac{1+P_{Cell}}{2}) + (\frac{1-P_{SM}}{2})(\frac{1-P_{Cell}}{2})] \tag{44}$$

$$T^{Expt}_{(\downarrow\uparrow)} = \sigma^{NSF}[(\frac{1-P_{SM}P_F}{2})(\frac{1+P_{Cell}}{2}) + (\frac{1+P_{SM}P_F}{2})(\frac{1-P_{Cell}}{2})] \tag{45}$$

Using the definition of P_{Cell} from Eqn. 36 we get

$$F.R._{^3He\uparrow}^{Expt} = \frac{T_{(\uparrow\uparrow)}^{Expt} - T^{Blocked\ Beam}}{T_{(\downarrow\uparrow)}^{Expt} - T^{Blocked\ Beam}} = \frac{1 + tanh(\mu\wp_{^3He})P_{SM}}{1 - tanh(\mu\wp_{^3He})P_{SM}P_F} \tag{46}$$

$$\wp_{3He}(t_n) = \frac{1}{\mu} tanh^{-1}\left[\frac{F.R._{^3He\uparrow}^{Expt} - 1}{P_F F.R._{^3He\uparrow}^{Expt} + 1}\left(\frac{1}{P_{SM}}\right)\right] \tag{47}$$

Similarly, with the ^{3}He oriented $\downarrow$ we get,

$$T_{(\downarrow\downarrow)}^{Expt} = \sigma^{NSF}[(\frac{1 + P_{SM}P_F}{2})(\frac{1 + P_{Cell}}{2}) + (\frac{1 - P_{SM}P_F}{2})(\frac{1 - P_{Cell}}{2})] \tag{48}$$

$$T_{(\uparrow\downarrow)}^{Expt} = \sigma^{NSF}[(\frac{1 - P_{SM}}{2})(\frac{1 + P_{Cell}}{2}) + (\frac{1 + P_{SM}}{2})(\frac{1 - P_{Cell}}{2})] \tag{49}$$

$$F.R._{^3He\downarrow}^{Expt} = \frac{T_{(\downarrow\downarrow)}^{Expt} - T^{Blocked\ Beam}}{T_{(\uparrow\downarrow)}^{Expt} - T^{Blocked\ Beam}} = \frac{1 + tanh(\mu\wp_{^3He})P_{SM}P_F}{1 - tanh(\mu\wp_{^3He})P_{SM}} \tag{50}$$

$$\wp_{3He}(t_n) = \frac{1}{\mu} tanh^{-1}\left[\frac{F.R._{^3He\downarrow}^{Expt} - 1}{P_F + F.R._{^3He\downarrow}^{Expt}}\left(\frac{1}{P_{SM}}\right)\right] \tag{51}$$

Thus, as long as have measured P_{SM} for each sample condition (this may be field and temperature dependent), and we can make the assumption that the sample scattering contribution to the measured transmission is negligible (i.e. a significant amount of long-range, low-Q scattering isn't present), we can use the flipping ratios to measure $\wp_{3He}(t_n)$. From this we can extract Γ as an exponential decay (Eqn. 43), same as in the final step of Method B. A rough test regarding the assumption of negligible low-Q sample scattering is to check whether the measured flipper polarization changes as a function of condition-varied, sample depolarization (if present) using equations 39 and 42. The flipper polarization should only depend on the neutron wavelength, so if P_F does change with varied sample depolarization (P_{SM}) you might need to consider the effect of non-negligible sample scattering into your measured transmission files.

F.4 Recap of Approaches

NMR is the best option when it can be applied. If the stray fields at the ^{3}He cell are too great to use NMR, then approaches B and C should be considered. B utilizes an unpolarized beam, and it is valid as long as the sample doesn't *polarize* the beam. Method C utilizes a series of polarized beam flipping ratios, and it is valid as long as the low-Q sample scattering is negligible in comparison with the measured transmission. Both B and C should be exact when the sample is removed from the beam.

Appendix G Measurement of ^{3}He cell's glass transmission and opacity

T_E, the transmission of an unfilled cell, and neutron attenuation length or opacity, μ are typically known very well for each ^{3}He cell. They can be measured directly, however, using the following equation,

$$T_E e^{-\mu} = \frac{T_{\textit{depolarized cell, unpolarized beam}} - T_{\textit{blocked, unpolarized beam}}}{T_{\textit{empty, unpolarized beam}} - T_{\textit{blocked, unpolarized beam}}}. \tag{52}$$

Since T_E is not be expected to change with time (and was measured well before the cell with first filled with helium), it is more common to check that the value of μ isn't drifting over time.

References

[1] Hildebrandt B et al. 2002 *Crit.Rev.Oncol.Hematol.* **43** 33–56

[2] Hilger I, Hergt R and Kaiser W A 2007 IEE Proc., *Nanobiotechnol.* **152** 33–9

[3] DeNardo S J, DeNardo G L, Natarajan A, Miers L A, Foreman A R, Gruettner C, Adamson G N and Ivkov R 2007 *J. Nucl. Med.* **48** 437–44

[4] Hoopes P J etal 2007 *Proc.SPIE* **6440** 64400K

[5] Johannsen M etal 2007 *Int.J.Hyperth.* **23** 315–23

[6] Dewhirst M W, Jones E, Samulski T, Vujaskovic Z, Li C and Prosnitz L 2003 *Cancer Medicine 6th edn*, ed D W Kufe, R E Pollock, R R Weichselbaum, R C Bast Jr and T S Gansler (Hamilton: Decker) pp 623–36

[7] vanderZee J 2002 *Ann.Oncol.* **13** 1173–84

[8] DeNardo S J, DeNardo G L, Miers L A, Natarajan A, Foreman A R, Gruettner C, Adamson G N and Ivkov R 2005 *Clin. Cancer Res.* **11** 7087s–92s

[9] Corot C, Robert P, Ideé J-M and Port M 2006 *Adv. Drug Deliv. Rev.* **58** 1471–504

[10] Artemov D,Bhujwalla Z M and Bulte J W M 2004 *Curr. Pharm. Biotechnol.* **5** 485–94

[11] Hadjipanayis C G,Bonder M J,Balakrishnan S,Wang X, Mao H and Hadjipanayis G C 2008 *Small* **4** 1925–9

[12] Rosensweig R E 2002 *J. Magn. Magn. Mater.* **252** 370–4

[13] Bourrinet P,Bengele H H,Bonnemain B,Dencausse A, Ideé J-M, Jacobs P M and Lewis J M 2006 *Invest. Radiol.* **41** 313–24

[14] Tsuji J S,Maynard A D,Howard P C,James J T,Lam C, Warheit D B and Santamaria A B 2006 *Toxicol. Sci.* **89** 42–50

[15] Eggeman A S,Majetich S A,Farrell D and Pankhurst Q A 2007 *IEEE Trans. Magn.* **43** 2451–3

[16] Adair E R and Black D R 2003 *Bioelectromagn.Suppl.* **6** S17–38

[17] Owens D E III and Peppas N A 2006 *Int. J. Pharm.* **307** 93–102

[18] Majewski P and Thierry B 2007 *Crit.Rev.Solid State Mater. Sci.* **32** 203–15

[19] Gupta A K, Naregalkar R R, Vaidya V D and Gupta M 2007 *Nanomedicine* **2** 23–39

[20] Ivkov R, DeNardo S J, Daum W, Foreman A R, Goldstein R C, Nemkov V S and DeNardo G L 2005 *Clin. Cancer Res.* **11** 7093s–103s

[21] Dennis C L et al 2009 *Nanotechnology* **20** 395103

[22] Dennis C L, Jackson A J, Borchers J A, Ivkov R, Foreman A R, Goernitz E, Lau J W and Gruettner C 2008 *J. Appl. Phys.* **103** 07A319

[23] Dennis C L et al 2008 *J. Phys. D: Appl. Phys.* **41** 134020

[24] Sears, V.F. 1992 *Neutron News* **3**, 29-37

[25] http://www.ncnr.nist.gov/resources/index.html

[26] Details regarding the ^{3}He cells can be found at: http://www.ncnr.nist.gov/equipment/he3nsf/index.html

[27] Glinka C, Barker J,Hammouda B, Krueger S, Moyer J and Orts W 1998 *J. Appl. Cryst.* **31**, 430.

[28] R. M. Moon, T. Riste, and W. C. Koehler, Polarization Analaysis of Thermal Neutron Scattering, *Physical Review* **181** 920 (1969).

[29] K. L. Krycka, R. A. Booth, C. R. Hogg, Y. Ijiri, J. A. Borchers, W. C. Chen, S. M. Watson, M. Laver, T. R. Gentile, L. R. Dedon, S. Harris, J. J. Rhyne, and S. A. Majetich, Core-Shell Magnetic Morphology of Structurally Uniform Magnetite Nanoparticles, accepted to *Physical Review Letters* (2010)